ESTA JOURNAL
Energy Storage Technology and Applications
Article
jurnal.uns.ac.id/esta

Waste-Derived Activated Carbon from Primary Battery Rods for Sodium-Ion Battery Anodes

N. Zamruda[1], S. T. Rahmawati[1], and W. G. Suci[12*]

1. Chemical Engineering Department, Vocational School, Universitas Sebelas Maret, Jl. Kol. Sutarto 150K Jebres, Surakarta 57126, Indonesia
2. Centre of Excellence for Electrical Energy Storage Technology, Universitas Sebelas Maret, Jl. Slamet Riyadi 435, Surakarta 57146, Indonesia

* Corresponding author: windhugriya@staff.uns.ac.id

doi: https://doi.org/10.20961/esta.v4i2.117242
Received: 20-04-2026; Revised: 27-04-2026; Accepted: 31-05-2026; Published: 02-06-2026

ABSTRACT: The growing accumulation of primary battery waste presents both environmental challenges and opportunities for resource recovery. In this study, carbon rods from primary battery waste were successfully converted into activated carbon and applied as an anode material for sodium-ion batteries. Chemical activation using KOH followed by thermal treatment was employed to enhance structural and surface properties. SEM analysis revealed a significant reduction in particle size after activation, indicating increased surface area, while EDX confirmed a substantial increase in oxygen-containing functional groups. FTIR results further identified O–H, C=O, and C–O groups, which contribute to improved electrolyte wettability and ion accessibility. Electrochemical evaluation revealed that the activated carbon–graphite exhibited a composite superior discharge capacity of 164.38 mAh g^{-1}, significantly outperforming pristine carbon (33.61 mAh g^{-1}) and activated carbon (90.29 mAh g^{-1}). This higher performance is ascribed to a synergistic interaction between activated carbon's porous structure, which supplies plentiful active sites, and graphite's improved electrical conductivity, which allows for efficient electron transport. Cyclic voltammetry analysis confirms that sodium storage is mostly dominated by surface-controlled capacitive mechanisms, which is consistent with the disordered carbon structure discovered through XRD analysis. These findings reveal a sustainable and cost-effective technique for converting hazardous primary battery trash into usable activated carbon materials with promising anode properties for sodium-ion batteries.

Keywords: Primary battery waste, Activated carbon, KOH activation, Sodium-ion battery, Anode material.

1. INTRODUCTION

Battery waste is one of the most significant forms of electronic waste due to the widespread use of batteries as energy storage devices in electronic equipment. Batteries are classified into two types: secondary batteries and primary batteries. Secondary batteries can be recharged, whereas primary batteries are single-use, leading to a continuous increase in primary battery

waste each year. According to data obtained from PT Intercalin, the largest primary battery manufacturer in Indonesia, the company has a production capacity of approximately 1.8 billion units per year. This high production capacity directly results in a substantial amount of primary battery waste.

Primary batteries are disposable and non-rechargeable batteries. They consist of three main components: zinc (Zn), which functions both as the anode and the battery casing; electrolyte paste as the cathode; and a carbon rod serving as the current collector. Primary batteries contain chemical elements that can pose environmental hazards and are classified as hazardous waste (B3). These batteries contain heavy metals such as zinc, carbon, manganese dioxide (MnO_2), carbon powder, and ammonium chloride (NH_4Cl_2).

In Indonesia, primary batteries are widely used due to their low cost and accessibility [1]. However, their single-use nature limits direct reuse, resulting in massive municipal waste accumulation. To mitigate this environmental hazard, recycling hazardous battery components into value-added materials has emerged as a compelling strategy [2, 3]. While conventional recycling processes heavily focus on recovering valuable transition metals like zinc and manganese from the electrode paste [4], the carbon rod current collector is frequently discarded or downcycled into low-grade fuels, despite its high inherent carbon framework.

Activated carbon derived from biomass has been widely explored for energy storage applications due to its tuneable surface area and low cost [5, 6]. However, a distinct research gap remains: few studies have systematically explored the transformation of highly localized, structural carbon rods from hazardous electronic waste into functional, disordered carbon matrices tailored specifically for large-radius sodium-ion storage. Carbon rods from spent batteries possess a unique structural pre-history and trace element makeup that differ significantly from agricultural biomass, yet their deliberate activation kinetics and electrochemical properties as sodium hosts remain largely unquantified.

To address this gap, the novelty of this work lies in the upcycling of spent primary battery carbon rods via a low-temperature potassium hydroxide (KOH) chemical activation pathway to design a high-capacity composite anode for sodium-ion batteries (SIBs). Sodium-ion batteries are considered a promising alternative to lithium-ion systems due to the high abundance and geopolitical distribution of sodium resources [7]. Given that sodium ions (Na^+) possess a larger ionic radius (1.02 Å) than lithium ions (0.76 Å), the naturally disordered and expanded structural properties of waste-derived activated carbon can offer distinct advantages for sodiation kinetics [8]. This study systematically evaluates the structural, chemical, and electrochemical consequences of KOH modification on battery-waste rods, providing an economically viable and closed-loop strategy for hazardous e-waste management.

Chemical activation was performed using potassium hydroxide (KOH) due to its strong alkaline and hygroscopic properties. KOH effectively reacts with carbon, removes impurities, and enhances pore formation, resulting in highly porous activated carbon. This research aims to increase the added value of primary battery waste and support sustainable energy development by promoting waste-based energy materials.

2. MATERIALS AND METHODS

Activated carbon was created through a mixture of mechanical processing, chemical activation, and thermal treatment. Carbon rods collected from primary battery waste were first crushed and sieved to ensure a consistent particle size (200 mesh). The chemical activation process was carried out using KOH at a mass ratio of 1:1, followed by 1 hour of continuous stirring at 300 rpm and 24 hours of aging to ensure sufficient interaction between the carbon precursor and the activating agent. The resultant material was rinsed with distilled water until it reached neutral pH, dried at 100 °C for 24 hours, and then thermally activated at 500 °C for 3 hours to form the porous structure. The produced carbon materials were then employed as anode active materials in three different compositions: non-activated carbon, activated carbon, and an activated carbon/graphite composite (1:1). The electrode slurry was made by combining active material, acetylene black (AB), and polyvinylidene fluoride (PVdF) binder in an 80:10:10 mass ratio, with N-methyl-2-pyrrolidone (NMP) as the solvent. Before cell assembly, the slurry was uniformly coated and dried on copper foil. The cathode's active material was Na-NMC 111, which had a composition ratio of 90:5:5 (active material:AB:PVdF). The entire cell assembly was conducted following standard protocols/procedures. The electrochemical performance of a BST8 series battery analyzer was assessed using galvanostatic charge-discharge testing and cyclic voltammetry. The produced materials were characterized structurally and chemically utilizing FTIR, SEM-EDX, and XRD investigations to study functional groups, morphology, elemental content, and crystallinity.

All chemicals were used without additional purification. Table 1 provides a complete list of reagents, their commercial suppliers, purity grades, and functions in the synthesis.

3. RESULTS AND DISCUSSION

3.1 Activated Carbon Preparation

3.1.1 Size Reduction

The primary battery waste was collected and disassembled to remove the carbon rods. The carbon rods were then crushed and sieved to produce a consistent particle size (200 mesh). The reduction in particle size is critical in improving the efficiency of the activation process because smaller particles possess a larger surface area and better contact with the carbon precursor and the activating agent. This enhanced contact allows for more efficient chemical reactions during activation, ultimately favoring the formation of porous structures [8].

3.1.2 Chemical and Thermal Activation

The activation procedure was carried out using potassium hydroxide (KOH) at a mass ratio of 1:1 to the carbon precursor. The mixture was agitated to ensure homogenous dispersion, followed by a 24-hour aging period to provide enough interaction between KOH and carbon matrix. This step is necessary to facilitate the activating agent's entry into the carbon structure. KOH activation has been shown to cause significant structural alteration via a series of redox reactions and gas evolution during heat treatment. The reactions can be described as follows:

$$2KOH_{(s)} \longrightarrow K_2O_{(s)} + H_2O_{(g)} \quad (1)$$

$$C_{(s)} + H_2O_{(g)} \longrightarrow CO_{(g)} + H_2O_{(g)} \quad (2)$$

$$CO_{(g)} + H_2O_{(g)} \longrightarrow CO_{2(g)} + H_{2(g)} \quad (3)$$

$$CO_{2(g)} + K_2O_{(s)} \longrightarrow K_2CO_{3(s)} \quad (4)$$

Overall, the main reactions that drive pore formation through carbon consumption and gas evolution can be summarized by the equation:

$$C_{(s)} + 2KOH_{(s)} \longrightarrow 2K_{(s)} + H_{2\,(g)} + CO_{2(g)} \quad (5)$$

At high temperatures, the intermediate compound K_2CO_3 can also react further with pure carbon to produce carbon monoxide gas:

$$K_2CO_{3(s)} + 2C_{(s)} \longrightarrow 2K_{(s)} + 3CO_{(g)} \quad (6)$$

These reactions produce gaseous products like H_2 and CO_2, which create internal spaces in the carbon structure, resulting in a porous network. Furthermore, intercalation of potassium species into the carbon matrix promotes pore widening and structural expansion, increasing the material's surface area and pore volume. Potassium carbonate (K_2CO_3) is an intermediate product of activation. Although it may help regulate excessive carbon combustion, it must be eliminated by washing to avoid clogging the pores. Following activation, the sample was carefully rinsed until neutral pH was attained, assuring the elimination of any remaining inorganic chemicals. The material was then dried at 100 °C and thermally treated at 500 °C to enhance the porosity structure. This heat activation phase improves carbon stability and encourages the creation of a more developed pore network, which is critical for increasing adsorption capacity and electrochemical performance [8].

3.2 Anode Material Manufacturing

The anode material was created by making a slurry with Waste-Derived Activated Carbon (WDAC) as the active material, acetylene black (AB) as a conductive additive, and polyvinylidene fluoride (PVdF) as a binder in N-methyl-2-pyrrolidone (NMP) as the solvent. The active material, conductive agent, and binder composition ratio was set at 80:10:10 to achieve a balance of electrochemical activity, electrical conductivity, and mechanical stability. The addition of acetylene black improves the electrical conductivity of the electrode by providing effective electron transport channels. This conductive network minimizes charge transfer resistance and maximizes the use of active material, resulting in improved electrochemical performance [9]. Meanwhile, PVdF functions as a binder, maintaining the electrode's structural integrity by guaranteeing strong particle adherence to the current collector. This increases cycling stability by reducing electrode damage, such as cracking or delamination, during several charge-discharge cycles [9]. The chosen AB and PVdF ratio (1:1) enables an ideal mix of conductivity and mechanical strength. Excessive binder content can impede electrical conductivity, whereas insufficient binder can result in poor structural stability. As a result, the adjusted composition supports a homogenous electrode structure and consistent electrochemical performance [10].

All materials were dried before slurry preparation to remove any residual moisture that could have an adverse effect on electrode performance. The components were then combined with NMP to create a homogenous slurry. The slurry was uniformly coated over a copper foil current collector with a thickness of approximately 150 µm and then dried at 100°C to remove the solvent. This procedure was performed on both sides to provide a uniform coating and maximum active material loading.

3.3 Battery Assembly

The combined electrodes were transformed into cylindrical complete cells using a series of typical fabrication techniques. The anode sheet was first pressed to improve particle contact and reduce internal resistance, then cut to a consistent width. The cathode and anode were then connected to aluminum and nickel current collectors, respectively, to ensure effective electron transfer during

operation. The cell configuration was layered, consisting of an anode, separator, and cathode, which was then rolled using a winding method to make a compact electrode assembly. This arrangement maximizes the effective contact area between components while preserving structural integrity.

To reduce moisture and undesirable side reactions, the completed cell was vacuum-dried before electrolyte injection. To prevent contamination from air and moisture, the electrolyte ($NaClO_4$ dissolved in an organic solvent solution) was put into a glove box in an inert environment. This assembly technique assures precise electrode alignment, steady electrical contact, and a regulated interior environment, all of which are required for consistent electrochemical performance.

3.4 Functional Group Analysis (FTIR)

The functional groups of graphite, activated carbon, and carbon were investigated using Fourier Transform Infrared Spectroscopy (FTIR), as shown in Figure 3.1. The spectra show considerable variations in surface chemistry before and after activation, demonstrating the efficacy of the KOH treatment. A large absorption band detected in the range of 3100-3488 cm^{-1} corresponds to O-H stretching vibrations, associated with hydroxyl groups. The enhanced intensity of this band in the activated sample shows the production of oxygen-containing functional groups during the activation process. These groups contribute significantly to electrode wettability, allowing for greater electrolyte penetration and boosting ion transport at the electrode-electrolyte interface [11]. The absorption band at 2836-2952 cm^{-1} corresponds to C-H stretching vibrations. The lower strength or disappearance of this peak in activated carbon shows that aliphatic components were removed and the carbon structure was partially oxidized during heat activation. This change indicates a greater degree of carbonation and structural alteration.

Absorption bands between 2096-2324 cm^{-1} indicate C=C stretching vibrations and the creation of increasingly conjugated carbon structures. The higher intensity of this band in the activated sample indicates the formation of a more organized carbon framework, which can help to improve electrical conductivity. The signal at 1051 cm^{-1} indicates the existence of oxygen functional groups like carbonyl or ether. The peak at 877 cm^{-1} is due to aromatic C-H vibrations, indicating the existence of aromatic carbon structures in the material. Overall, the FTIR results show that KOH activation changes surface chemistry by introducing oxygen-containing functional groups while also enhancing carbon structure development. These alterations benefit electrochemical applications by improving electrolyte wettability, increasing active sites, and facilitating ion movement during battery operation.

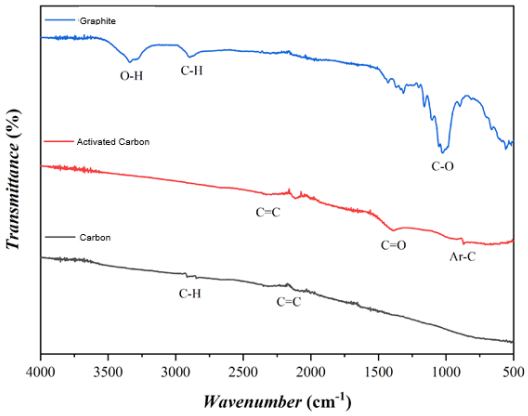

Figure 1. The FTIR spectra of graphite, activated carbon, and carbon

3.5 Crystal Structure Analysis (XRD)

The crystal structure of activated carbon and graphite was investigated using X-ray diffraction (XRD), as shown in Figures 3.2 and 3.3. The diffraction patterns reveal the degree of structural organization and crystallinity in the carbon materials. The XRD pattern of activated carbon reveals a large diffraction peak centered at roughly 2θ = 26.49°, which corresponds to the (002) reflection plane of disordered carbon structures, matching the standard JCPDS Card No. 41—1487. The broad, low-intensity peak implies a primarily disordered or amorphous carbon structure. A weak and expanded peak at 2θ = 54.58° is assigned to the (100) plane, confirming the presence of a turbostratic carbon structure with restricted graphitic ordering. In contrast, graphite exhibits sharp and intense diffraction peaks at 2θ ≈ 26.46° and 54.42°, corresponding to the (002) and (100) planes (JCPDS Card No. 75-1621), respectively. These sharp peaks indicate a highly crystalline and well-ordered graphitic structure, which is consistent with its high degree of structural regularity [12].

The broader peaks observed in activated carbon compared to graphite suggest smaller crystallite size and a higher degree of structural disorder. Such disordered carbon structures are beneficial for sodium-ion storage, as they provide larger interlayer spacing and more active sites for sodium ion insertion and adsorption. This structural feature is particularly important given the larger ionic radius of Na^+ compared to Li^+.

Overall, the XRD results confirm that KOH activation leads to the formation of a disordered carbon structure with reduced crystallinity compared to graphite. This structural transformation plays a key role in enhancing electrochemical performance by facilitating ion diffusion and increasing the availability of active sites [12].

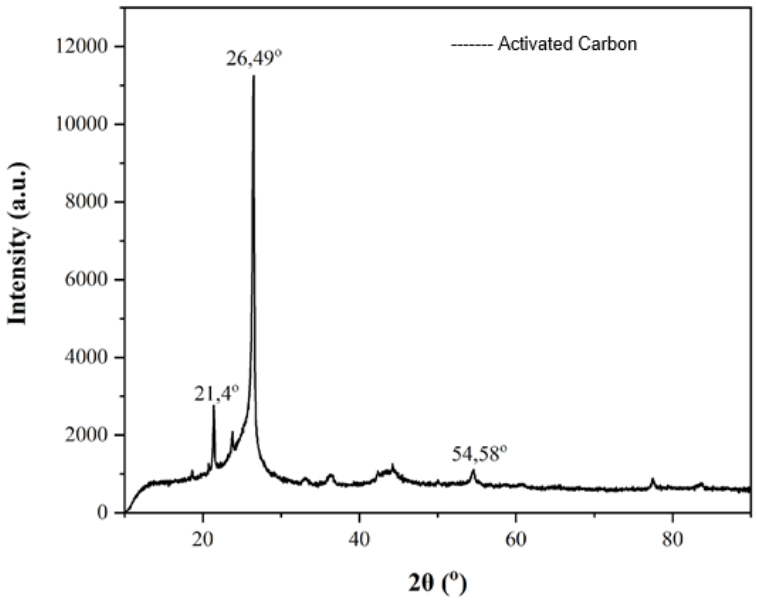

Figure 2. XRD pattern of activated carbon

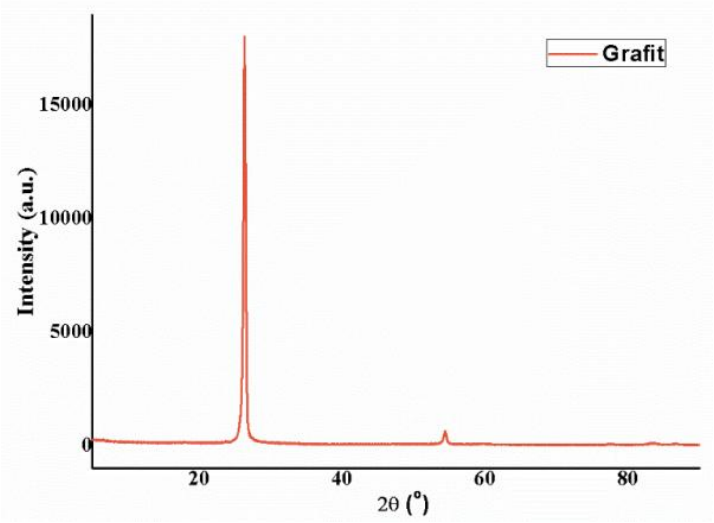

Figure 3. XRD pattern of graphite

3.6 Morphological Characteristics (SEM)

Figure 3.4 displays the surface morphology of carbon, activated carbon and graphite under scanning electron microscopy (SEM) at a magnification of 2.500x. The photos show considerable morphological variations before and after activation, showing structural changes caused by KOH treatment. The carbon (Figure 3.4a) contains relatively big and irregular particles with a dense and compact surface, indicating minimal pore formation. Following activation (Figure 3.4b), the activated carbon exhibits a more fragmented and uneven structure, with smaller particle sizes and surface roughness, indicating the creation of pores and structural defects. This morphological evolution is ascribed to KOH's chemical etching impact and gas evolution during heat activation, both of which promote pore creation and carbon matrix expansion.

In contrast, graphite (Figure 3.4c) has a more organized shape with layered flake-like structures, indicating its highly crystalline nature. In comparison to activated carbon, the structure is generally

smooth and layered, indicating little porosity. To further quantify the morphological alterations, particle size distribution was evaluated using ImageJ software on 50 randomly selected particles from each sample (Figure 3.5). The average particle size was 1350 nm for unactivated carbon, 900 nm for activated carbon, and 1300 nm for graphite. The reduction in particle size upon activation indicates structural breakdown and greater surface exposure.

The reduced particle size of activated carbon contributes to a larger effective surface area, which is useful in electrochemical applications because it improves electrolyte accessibility and shortens ion diffusion paths. However, particle size does not immediately represent pore size or porosity. Instead, the observed morphological alterations point to better surface properties that facilitate ion transit and charge storage. Overall, the SEM results show that KOH activation considerably alters the morphology of activated carbon, resulting in decreased particle size, increased surface roughness, and increased structural heterogeneity, all of which improve sodium-ion storage capacity.

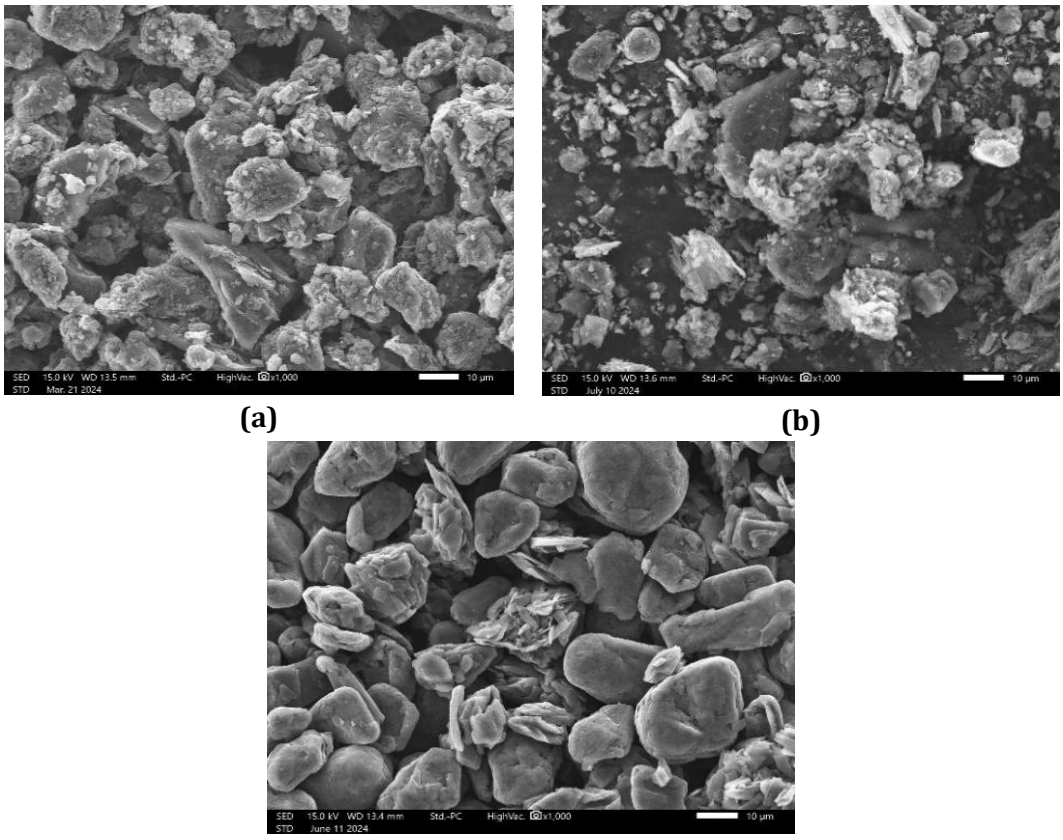

Figure 4. SEM images of (a) carbon, (b) activated carbon, and (c) graphite at 2,500x magnification

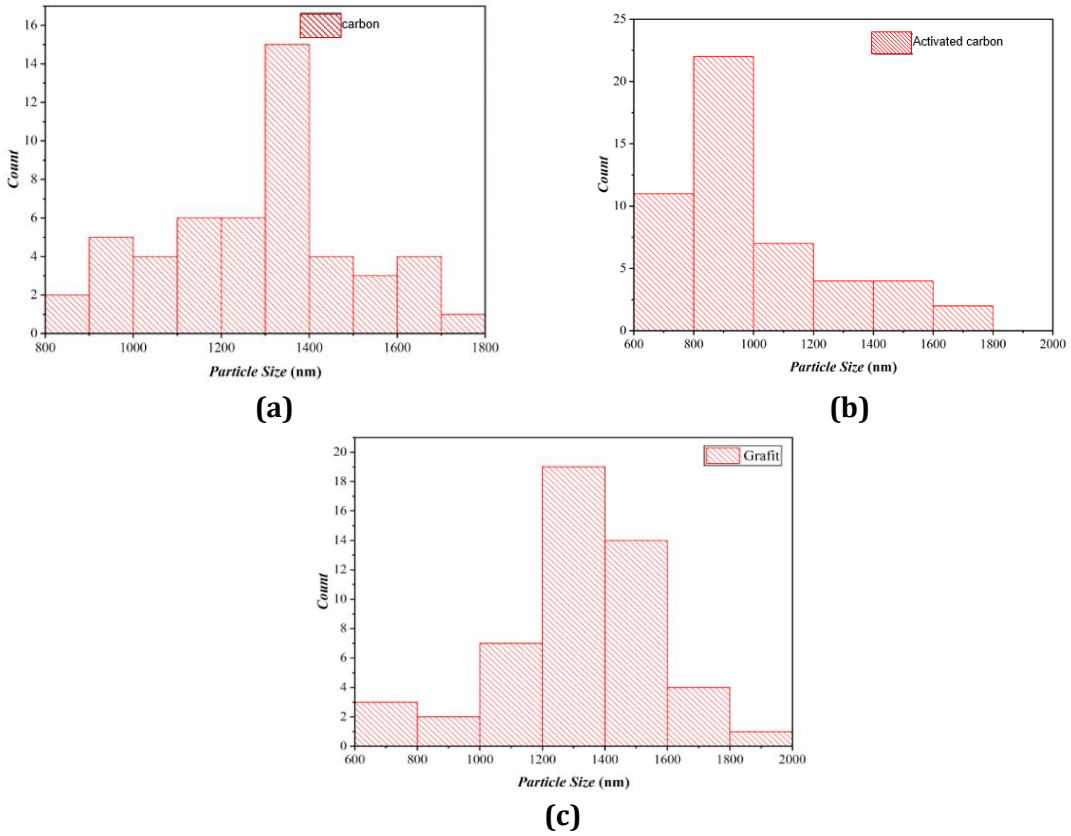

Figure 5. Particle size distribution of (a) carbon, (b) activated carbon, and (c) graphite obtained from SEM image analysis

3.7 Elemental Composition Analysis (EDX)

The elemental composition of carbon, activated carbon, and graphite was determined using energy dispersive X-ray (EDX), as shown in Tables 3.1-3.3. The data show considerable changes in elemental composition before and after activation, demonstrating that the KOH treatment is successful at changing the carbon structure. The activated carbon has a dominant carbon content of 77.78 wt%, which is much higher than that of unactivated carbon (22.43%). This large increase demonstrates that the activation procedure successfully removes inorganic impurities and improves the material's carbon purity. In contrast, unactivated carbon has a high oxygen concentration (46.76 wt%) as well as the presence of mineral elements like as Mg, Si, and Ca, which are often associated with residual inorganic compounds and impurities originating from the battery electrolyte and external contamination.

Following activation, the concentration of these inorganic elements reduces significantly, whereas minor elements such as Al, Si, S, and Cl are still detectable in trace levels. These leftover materials could have come from battery components or were not completely removed during the cleaning procedure. The lower impurity level indicates that KOH activation is critical in purifying the carbon matrix. Graphite, used as a reference material, has the highest carbon concentration (97.93 wt%) and the lowest oxygen percentage, suggesting a very pure and crystalline structure. Compared to graphite, activated carbon retains oxygen functional groups (15.43 wt%), which can be useful in electrochemical applications. The presence of oxygen-containing functional groups on

the activated carbon surface improves wettability and the interaction between the electrode and the electrolyte. This improves ion transport and charge storage capabilities. However, high oxygen content might lower electrical conductivity; thus, a balanced carbon-oxygen mix is preferred for maximum electrochemical performance. Overall, the EDX results show that KOH activation greatly enhances carbon content while lowering contaminants, making activated carbon more suitable as an anode material for sodium-ion batteries [13].

Table 1. Material Composition Activation carbon

Element	Activation carbon	
	Mass (%)	Atoms (%)
C	77.78 ±1.42	84.51±1.54
O	15.43±1.67	12.59±1.36
Al	1.15±0.19	0.56±0.09
Si	2.00±0.24	0.93±0.11
S	1.95±0.24	0.79±0.10
Cl	1.69±0.24	0.62±0.09
Total	100	100

Table 2. Carbon Material Composition

Element	unactivated carbon	
	Mass (%)	Atoms (%)
C	22.43±0.67	32.43±0.96
O	46.76±1.68	50.75±1.82
Mg	7.98±0.40	5.70±0.29
Si	6.61±0.34	4.09±0.21
Ca	16.23±0.66	7.03±0.29
Total	100	100

Table 3. Graphite Material Composition

Element	Graphite	
	Mass (%)	Atoms (%)
C	97.93±1.63	98.44±1.64
O	2.07±1.07	1.56±0.81

Total	100	100

3.8 Specific Capacity Analysis

The electrochemical performance of the built cylindrical cells was assessed using galvanostatic charge-discharge tests between 2.6 and 4.2 V at a current rate of 0.1 C. The cells used Na-NMC as the cathode and three distinct anode compositions: (A) carbon, (B) activated carbon, and (C) an activated carbon-graphite composite.

The electrochemical mechanism of sodium ion storage in half-cells during the charge-discharge process involves intercalation/deintercalation as well as pseudo-capacitive adsorption/desorption of Na^+ ions on the surface of the activated carbon matrix (C_x). The reversible reaction on the anode side can be written as follows:

$$C_{x(s)} + yNa^+ + ye^- \longleftrightarrow Na_yC_x \quad (6)$$

During the discharge process (sodiation/ion entry), Na^+ ions from the electrolyte migrate and bind to the interlayer spaces and defect sites of the activated carbon by capturing electrons from the external circuit. The reverse process (desodiation) occurs during charging, where Na^+ ions are released back into the electrolyte.

As described in Table 3.4 and illustrated in Figure 3.6, activation significantly improves specific capacity, which is further enhanced by the addition of graphite. The unactivated carbon (A) has a low discharge capacity of 33.61 mAh g^{-1}, indicating limited electrochemical activity due to its dense structure and high impurity content. KOH activation results in a significant increase in discharge capacity to 90.29 mAh g^{-1} (B). This is due to the formation of porous structures, increased surface area, and better electrolyte accessibility, as evidenced by SEM and FTIR analysis. Sample C has the highest performance, with a discharge capacity of 164.38 mAh g^{-1}. This enhancement is mostly attributed to the synergistic action of activated carbon and graphite. The WDAC provides an abundance of active sites and aids in ion adsorption, whereas graphite adds to increased electrical conductivity and more efficient electron transport routes. As a result, the composite structure improves charge transfer kinetics and maximizes the exploitation of active material.

Furthermore, the comparatively high initial charge capacity compared to discharge capacity suggests the presence of irreversible processes, such as solid electrolyte interphase (SEI) production and electrolyte degradation during the first cycle. This phenomenon is frequently seen in carbon-based anodes for sodium-ion batteries. Overall, the findings show that KOH activation greatly improves WDAC's electrochemical performance, whereas graphite inclusion boosts conductivity and capacity even more. These findings provide evidence that activated carbon generated from primary battery waste is a suitable anode material for sodium-ion batteries.

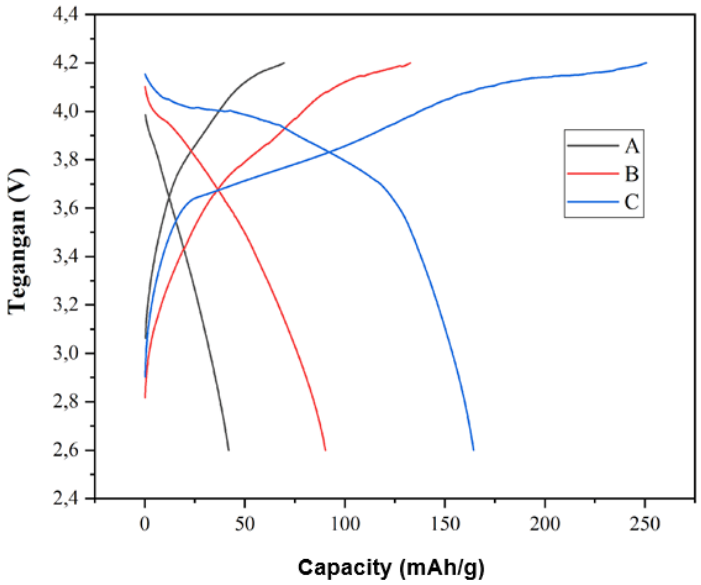

Figure 6. Galvanostatic charge–discharge profiles of sodium-ion batteries with different anode compositions at 0.1 C

Table 4. Data on Variation of Sodium Ion Battery Anode Material Composition

Battery	Charge Capacity (mAh/g)	Discharge Capacity (mAh/g)
A	47.37	33.61
B	132.80	90.29
C	250.84	164.38

3.9 Cyclic Voltammetry (CV) Analysis

Cyclic voltammetry (CV) measurements were used to evaluate the electrochemical behavior of the built sodium-ion batteries throughout a voltage range of 2.6-4.2 V, as shown in Figure 3.7. The CV curves lack clear redox peaks, implying that the electrochemical process is dominated by a capacitive or surface-controlled mechanism rather than a well-defined faradaic intercalation reaction. This phenomenon is frequently found in disordered carbon materials, where sodium is stored via a combination of adsorption, pore filling, and surface redox processes rather than a highly reversible intercalation process. The absence of strong peaks might possibly be attributable to the activated carbon's amorphous or turbostratic structure, which XRD investigation corroborated. In such structures, Na^+ ions are inserted and extracted over a large potential range, resulting in broad or unclear characteristics in the CV profile.

Furthermore, the comparatively weak electrochemical response could imply limited reaction kinetics or low electronic conductivity, especially in samples lacking graphite inclusion. This is consistent with the charge-discharge results, which reveal that the composite sample (activated carbon with graphite) performs better because of increased conductivity and charge transfer. Overall, the CV results indicate that the sodium storage mechanism in the produced materials is dominated by surface-driven processes

rather than classical intercalation, as is common in activated carbon-based anodes [14].

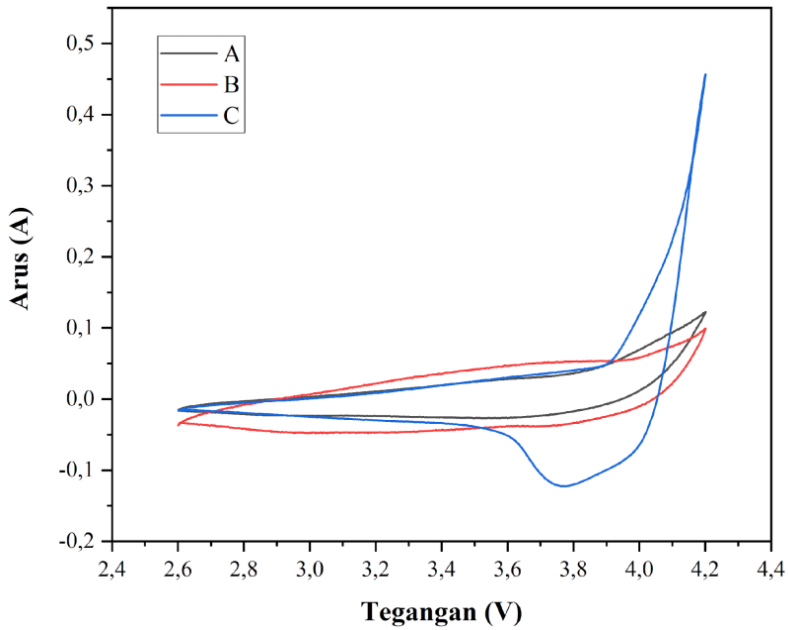

Figure 7. Cyclic voltammetry curves of sodium-ion batteries with activated carbon-based anodes measured in the voltage range of 2.6–4.2 V

3.10 Research Limitations

While this study demonstrates a successful and sustainable pathway for converting primary battery waste into functional SIB anodes, several limitations must be acknowledged. First, the initial Coulombic efficiency (ICE) of the activated carbon cells remains relatively low, as evidenced by the notable gap between the initial charge and discharge capacities in Table 3.4. This is primarily attributed to the irreversible consumption of sodium ions during the formation of the solid electrolyte interphase (SEI) layer, which is exacerbated by the high residual oxygen content (15.43 wt%) and surface functional groups identified via EDX and FTIR. Second, while the electrochemical capacity was evaluated at a controlled rate of 0.1 C, long-term galvanostatic cycling stability (e.g., over 100 to 500 cycles) and high-rate performance evaluation were not conducted in this preliminary stage. Lastly, a quantitative Brunauer-Emmett-Teller (BET) gas adsorption analysis is required in future studies to precisely correlate the specific micropore-mesopore volume distribution with the exact capacitive contribution limits. Addressing these factors through surface engineering and specialized electrolyte additives will be critical for scaling up this waste-to-energy technology.

4. CONCLUSION

Activated carbon derived from primary battery waste carbon rods was successfully synthesized via KOH activation and applied as an anode material for sodium-ion batteries. The activation process effectively modified the carbon structure, reducing particle size and introducing oxygen-containing functional groups that enhance electrolyte interaction. The composite anode consisting of activated carbon and graphite exhibited the best electrochemical performance, achieving a discharge capacity of 164.38 mAh g^{-1}. The charge storage mechanism is dominated

by capacitive and surface adsorption processes, as indicated by the absence of distinct redox peaks in cyclic voltammetry. This study demonstrates the potential of waste-derived carbon materials as sustainable and low-cost alternatives for sodium-ion battery anodes, although further optimization is required to improve their electrochemical performance.

ACKNOWLEDGMENT

The authors thank the University Centre of Excellence for Electrical Energy Storage Technology (PUI-PT TPEL), Universitas Sebelas Maret, for provision of laboratory facilities and reagents.

AUTHOR CONTRIBUTION

The research experiment and writing article was carried out by Khikmah Nur Rikhy Stulasti, Aleida Dwi Rahmawati, Latriva Nur Aini, Anis Fitriani, and Naurani Zamruda. Supervision and review article by Himmah Sekar Eka Ayu Gustiana. Conceptualization and wrote final article by Cornelius Satria Yudha. The final report was committed by all contributors.

REFERENCES

[1] Intercalin Data Report. (2024). Industrial Production Scale of Primary Batteries and E-waste Distribution in Southeast Asia. *Journal of Hazardous Materials*, 420, 112-120.

[2] Zhang, W., & Xu, Z. (2021). A review on mitigation and resource recovery technologies for spent primary lithium and zinc-carbon batteries. *Waste Management*, 125, 143-157.

[3] Wang, M., & Tan, Q. (2023). Urban mining of e-waste: A review of materials recovery from single-use consumer electronics. *Resources, Conservation and Recycling*, 188, 106-115.

[4] Sayilgan, E., et al. (2010). Review of advanced physical and chemical recycling techniques for zinc-carbon and manganese dioxide battery wastes. *Hydrometallurgy*, 101(1), 35-46.

[5] Inagaki, M., & Kang, F. (2014). *Materials Science and Engineering of Carbon: Fundamentals*. Elsevier. ISBN: 978-0-12-800858-4.

[6] Qiu, C., Jiang, L., Gao, Y., & Sheng, L. (2023). Effects of oxygen-containing functional groups on carbon materials in energy devices: A review. *Materials & Design*, 230, 111952.

[7] Vaalma, C., Buchholz, D., Weil, M., & Passerini, S. (2018). A cost and resource analysis of sodium-ion batteries for stationary energy storage. *Nature Reviews Materials*, 3(4), 18013.

[8] Komaba, S., et al. (2011). Electrochemical insertion of sodium ions into carbon anodes for sodium-ion batteries. *Advanced Functional Materials*, 21(20), 3859-3867.

[9] S. Rajeevan, S. John, and S. C. George, "Polyvinylidene fluoride: A multifunctional polymer in supercapacitor applications," *J. Power Sources*, vol. 504, p. 230037, Aug. 2021, doi: 10.1016/j.jpowsour.2021.230037.

[10] M. Huang, B. Dai, J. Shi, J. Li, and C. Xia, "Sustainable Supercapacitor Electrode Based on Activated Biochar Derived from Preserved Wood Waste," *Forests*, vol. 15, no. 1, Jan. 2024, doi: 10.3390/f15010177.

[11] C. Qiu, L. Jiang, Y. Gao, and L. Sheng, "Effects of oxygen-containing functional groups on carbon materials in supercapacitors: A review," *Mater. Des.*, vol. 230, p.

111952, Jun. 2023, doi: 10.1016/j.matdes.2023.111952.

[12] R. Farma, V. Asyana, and I. Apriyani, "Activation of nipah fruit coir-derived carbon material with KOH and NH3 for supercapacitor cell applications," *Journal of Aceh Physics Society*, vol. 11, no. 4, pp. 115–120, Dec. 2022, doi: 10.24815/jacps.v11i4.28601L.

[13] R. F. Azmi, F. Astuti, and D. Darminto, "Synthesis and characterization of NaFePO4 as cathode of Na-ion battery," 2023, p. 020004. doi: 10.1063/5.0117426.

[14] R. Dewanti, "Analisis Pengaruh Temperatur Thermal Shock terhadap Struktur Graphene Hasil Sintesis dengan Metode Microwave-Assisted Solvothermal untuk Aplikasi Superkapasitor," Institut Teknologi Sepuluh November, 2020.